Manchester Metropolitan University

https://e-space.mmu.ac.uk

{Mn$^{III}_2$Ln$^{III}_2$} (Ln = Gd, La or Y) butterfly complexes: ferromagnetic exchange observed between bis-μ-alkoxo bridged manganese(III) ions.

Kuduva R. Vignesh[a], Robert Martin[b], Gary Miller[b], Gopalan Rajaraman[a,*], Keith S. Murray[c,*], Stuart. K. Langley[b,*]

a) Department of Chemistry, Indian Institute of Technology Bombay, Mumbai-400076, India.

b) School of Science and the Environment, Division of Chemistry, Manchester Metropolitan University, Manchester, UK.

c) School of Chemistry, Monash University, Clayton, Victoria 3800, Australia.

Email: keith.murray@monash.edu (to handle correspondence), rajaraman@chem.iitb.ac.in and s.langley@mmu.ac.uk

Abstract

Three tetranuclear {Mn$^{III}_2$Ln$^{III}_2$} 'butterfly' complexes with common Mn$^{III}_2$ μ$_3$-alkoxo bridging motifs surrounded by two Ln^{III} ions (Ln = Gd, La or Y) have been studied by structural, magnetic and density functional theoretical calculations. The exchange coupling constant between the body-body Mn(III) ions is ferromagnetic in all cases, the La and Y examples being diamagnetic at the wing-wing positions. The wing-body J_{wb} (Mn-Gd) interaction is small and negative. Reasons are given for these J_{MnMn} values, including the effects of the terminal Ln^{III} ions, comparison to analogous Mn$_2$ dinuclears, and the effects of spin polarisation.

Keywords: mixed lanthanide-manganese(III) ions; ferromagnetic exchange; DFT; tetranuclear; spin polarisation

We dedicate this paper to Miguel Julve on the occurrence of his 65th birthday

Introduction

The magnetic properties of polymetallic coordination complexes, derived from transition and lanthanide metal ions continue to fascinate chemists and physicists alike [1,2]. The observation, for example, of magnetic hysteresis loops originating from a discrete molecule has been termed single-molecule magnetism (SMM), and is therefore of great technological importance as these molecular materials have the ability to store digital information by manipulating the orientation of the spin vector of the molecule with a magnetic field [3,4]. This property may lead to a greater density of data being stored, much greater than in current devices, however, drawbacks such as the operating temperature, which generally falls below 80 K must be overcome [5]. In practice a large number of factors influence the blocking/operating temperature, for example the spin ground state of the molecule, which is governed by the intramolecular magnetic exchange interactions. It is not a trivial task to design and synthesize polynuclear molecular coordination complexes with the desired exchange type (ferromagnetic vs antiferromagnetic) and exchange strength due to various synthetic limitations. This is readily apparent in the isolation of large polynuclear complexes using a self-assembly method of synthesis [6]. What can be useful, however, is the identification of common bridging motifs in complexes and analysing the effect that the type of metal ion, the bridging ligand, metal-metal distances, metal-ligand angles, for example, have on the nature and magnitude of the magnetic exchange parameter. Such a database can provide a starting point for the selection of metal ion and type of bridging ligand when designing experiments, which can result in the products relaying favourable magnetic properties.

An important ion in the search for new SMMs is Mn^{III}. This is due to its large number of unpaired electrons ($S = 2$) often resulting in a negative zero-field splitting parameter as desired for these SMMs. In order to design a SMM, it is preferable to have strong ferromagnetic exchange between neighbouring ions [4,7] and, thus, it is important to understand what controls the magnetic exchange interaction. Work in our group has focussed on developing magneto-structural correlations of the simplest building units i.e. dinuclear complexes to understand the influence various structural parameters has on the magnetic exchange interaction [8]. A recent study related to this work involved exchange data on dinuclear $\{Mn^{III}_2\}$ bridged via bis-μ-alkoxo ligands [8b,c]. The results revealed that the exchange was influenced by the orientation of the Jahn-Teller axes, with a

perpendicular orientation leading to a strong ferromagnetic exchange while, when it is parallel, an antiferromagnetic interaction occurs. This is not ideal as, in the ferromagnetic case, the perpendicular orientation of the Jahn-Teller (J-T) axes leads to a decrease in the anisotropy of the cluster, detrimental for designing SMMs. Following this work, and presented here, we have studied three new pseudo bis-μ-alkoxo {Mn^{III}_2} complexes, differing in the fact that the Mn^{III} ions are surrounded by diamagnetic Ln^{III} ions (Ln^{III} = La and Y (yttrium is considered a pseudo lanthanide ion due to its similarity in reactivity and size). We also present a complex where the lanthanide ion is paramagnetic (Ln^{III} = Gd) to see what influence this has on the magnetic exchange. The complexes presented have formulae $[Mn^{III}_2Ln^{III}_2(OMe)_2(hmp)_4(NO_3)_4(O_3SC_6H_4CH_3)_2]_n$ (where Ln = Gd (**1**), Y (**2**); hmpH = 2-hydroxy-methylpyridine) and $[Mn^{III}_2La^{III}_2(bdea)_2(bdeaH)_2(piv)_6]$ (**3**); bdeaH = N-butyldiethanolamine; piv = pivalate. Complexes **1** and **2** are newly synthesised, based on a method in our earlier report [9], whereas complex **3** was taken from the literature [10]. Interestingly, for **1 – 3** we find the J- T axes on the Mn^{III} ions are aligned parallel and the magnetic exchange interaction is ferromagnetic. To unambiguously model the magnetic exchange interactions and also to gain insight into the nature of the exchange coupling, we have employed theoretical calculations based on density functional theory (DFT) methods to study complexes **1–3**.

Materials and Methods

All reactions were carried out under aerobic conditions. Chemicals and solvents were obtained from commercial sources and used without further purification. Elemental analyses (CHN) were carried out by Campbell Microanalytical Laboratory, University of Otago, Dunedin, New Zealand. The syntheses of compounds **1** and **3** are as previously reported [9,10]

$[Mn^{III}_2Y^{III}_2(OH)(OMe)(hmp)_4(NO_3)_4(O_3SC_6H_4CH_3)_2]_n \cdot MeCN \cdot MeOH \cdot H_2O$ (2)

$Mn(NO_3)_2.4H_2O$ (1 mmol) and $Y(NO_3)_3.6H_2O$ (1 mmol) were dissolved in 20 mL of a 1:3 MeOH/MeCN solution. To this 2-hydroxymethylpyridine (1.5 mmol), p-toluenesulphonic acid (4 mmol) and triethylamine (5.5 mmol) was then added, resulting in a dark brown solution, which slowly turned purple after stirring for 4 hours. After this time the reaction was stopped and the solvent was allowed to evaporate slowly. After several days red/brown crystals of **2** had formed. Yield: 67 % (based on Mn) for **1**. Anal. Calculated (found) for

2·MeCN·MeOH·H$_2$O : $Mn_2Y_2C_{42}H_{51}O_{26}N_9S_2$: C, 34.80 (34.70); H, 3.55 (3.76); N, 8.70 (8.99). IR selected peaks; 1605(w), 1479(s), 1460(s), 1441(s), 1368(w), 1320(s), 1302(s), 1288(s), 1249(s), 1224(w), 1164(s), 1120(s), 1034(s), 1010(s), 815(w).

Powder X-ray diffraction

X-ray powder diffraction data were collected on a PANalytical X'Pert powder diffractometer using a Cu anode (Cu k$_{\alpha1}$ λ= 1.540598 Å) operating at 40 kV, 30 mA fitted with a PIXcel 1D detector operating in scanning line detector mode with a linear active length of 3.347° 2θ. Samples were prepared as flat powders and measured in reflection geometry in the range 5 - 100° 2θ with a step size of 0.013° 2θ. Data were processed using HighScore Plus version 4.0.

Magnetic measurements

Magnetic susceptibility measurements were carried out on a Quantum Design SQUID magnetometer MPMS-XL 7, which operated between 1.8 and 300 K for dc-applied fields that range from 0 – 5 T. Microcrystalline samples were dispersed in Vaseline in order to avoid torquing of the crystallites. The sample mulls were contained in a calibrated gelatine capsule held at the centre of a drinking straw that was fixed at the end of the sample rod. Alternating current (ac) susceptibilities were carried out under an oscillating ac field of 3.5 Oe with frequencies ranging from 0.1 to 1500 Hz.

Computational Details

The DFT calculations combined with the Broken Symmetry (BS) approach [11] have been employed to compute the magnetic exchange (*J*) values. The BS method has a proven record of yielding good numerical estimate of *J* constants for a variety of complexes [12]. This method has already been employed to compute reasonable estimates of exchange interactions (*J*) in numerous dinuclear as well as in polynuclear complexes earlier in our group including manganese [8,13] and {MnGd} clusters.[14] Here DFT calculations were performed using the B3LYP functional [15] with the *Gaussian 09* suite of programs [16]. The double-zeta quality basis set employing Cundari-Stevens (CS) relativistic effective core potential on Gd atom [17], LanL2DZ ECP basis set on La and Y [18] and Ahlrich's [19] triple-ζ-quality basis set for Mn as well as for the rest of the atoms. The energies of four spin configurations for **1** and energies of two spin configurations for **2** and **3** are computed to extract the exchange interactions [20]. The

computed spin configurations for **1** are given in the ESI (Table S1). Program PHI [21] was used for the simulation of magnetic susceptibilities and isothermal magnetizations.

Three exchange coupling constants for **1** and one exchange coupling for **2** and **3** are determined by DFT using B3LYP hybrid functional. In **1**, the following Hamiltonian is used to estimate the exchange interaction.
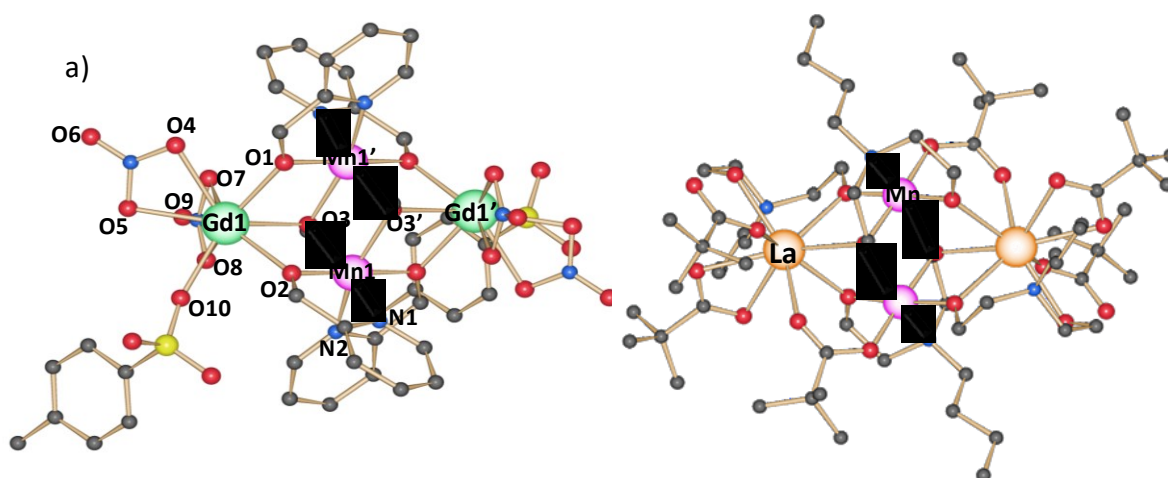
$$\hat{H} = -[2J_{wb}(S_{Mn1} S_{Gd1} + S_{Mn1} S_{Gd1'} + S_{Mn1'} S_{Gd1} + S_{Mn1'} S_{Gd1'}) + 2J_{bb}(S_{Mn1} S_{Mn1'}) + 2J_{ww}(S_{Gd1} S_{Gd1'})] \; Eq \; 1$$

Here J is the isotropic exchange coupling constant and S_{Mn} and S_{Gd} are spins on Mn^{III} (S= 2) and Gd^{III} (S=7/2) atoms respectively. In **2** and **3**, the following Hamiltonian is used to estimate the exchange interaction.

$$\hat{H} = -2J_{bb}(S_{Mn1} S_{Mn1'}) \; Eq \; 2$$

Results and discussion

Structural information

Fig. 1: (a) Molecular structure of **1** (Same applicable to **2**); (b) Molecular structure of **3** Mn^{III}, pink; Gd^{III}, green; La^{III}, orange;O, red; N, blue; C, black; S, yellow. The black bold bonds denote the Mn^{III} J-T axes which are elongated via O-Mn-N.

Full structural descriptions of the two motifs have been provided previously [9,10]. The identity and bulk purity of complex **2** was determined via powder X-ray diffraction (Fig. S1) and IR spectra (Fig. S2). **2** was found to be isostructural to **1**, as expected. The salient points relating to this work are as follows. Compounds **1 – 3 3** are heterometallic tetranuclear

complexes (Fig. 1), which display a butterfly or planar diamond type metallic core, with the Mn^{III} ions occupying the central body-body (bb) sites with the outer wing-wing (ww) sites occupied by Gd (**1**), Y (**2**) and La (**3**) ions. The Mn^{III} ions are bridged by two alkoxo ligands; methoxide in the case of **1** and **2** and ethoxide type for **3** - which is part of the N-n-butyldiethanolamine ligand. The two Mn^{III} ions are six coordinate, displaying J-T distorted octahedral geometries, which are axially elongated. The J-T axes in each case are aligned parallel (black bold bonds shown in Fig. 1) via (μ_3)O-Mn-N bonds and the bridging plane. Compounds **2** and **3** can be considered, magnetically, as {Mn$^{III}_2$} dinuclear complexes since the wing ions Y^{III} (**2**) and La^{III} (**3**) are diamagnetic. Selected bond lengths are given in the ESI (Table S2). We note that for **1** and **2** each complex is linked by sulphonate ligands forming 1D chains (Fig. S3).

Magnetic susceptibility measurements

Magnetic susceptibility measurements on compounds **1** and **2** were carried out in the 2 – 300 K temperature range, in an applied magnetic field of 1 T. Magnetic results for compound **3** were taken from the previously reported study.[10] The data are plotted as $\chi_M T$ versus temperature and shown in Figure 2. The room temperature $\chi_M T$ values of 21.6 cm^3 K mol^{-1} (**1**), 7.0 cm^3 K mol^{-1} (**2**) and 7.1 cm^3 K mol^{-1} (**3**) are higher than the expected value for two non-interacting Mn^{III} ions (in **2** and **3**, *viz.* 6 cm^3 K mol^{-1}) but similar for non-interacting Mn^{III} and Gd^{III} ions (in **1**, *viz.* 21.8 cm^3 K mol^{-1}), assuming $g = 2.0$. This is an indication of ferromagnetic exchange between the metal centres. Supporting this is the temperature dependent $\chi_M T$ profile which increases as the temperature is decreased, with maximum values observed for each complex revealing values of 22.8 cm^3 K mol^{-1}, 7.8 cm^3 K mol^{-1} and 10.5 cm^3 K mol^{-1} for **1** – **3** respectively. In order to quantify the exchange the $\chi_M T(T)$ data for **1** were fitted using the program PHI [21], using two coupling parameters; J_{bb} (Mn$^{III}\cdots$Mn^{III}) and J_{wb} (Gd$^{III}\cdots$Mn^{III} ions) and a single molecular g-factor. Intra- and inter-cluster Gd$\cdots$Gd interactions (Gd$\cdots$Gd distance = 6.3 Å (intra) and 6.0 Å (inter, via the sulfonate ligands)) are considered negligible and are ignored (see Fig. 3 for coupling scheme and Hamiltonian used). The best fit values were $J_{bb} = 1.72$ cm^{-1} and $J_{wb} = 0.014$ cm^{-1} (-2J convention) with $g = 2.00$ (Fig. 2, red line, FIT). These parameters result in an $S = 11$ ground state, with ten states ranging in value from $S = 0 – 10$, lying 1 cm^{-1} above the ground state. For complex **2** the $\chi_M T(T)$ data were fitted using a single coupling parameter; J_{bb} (Mn$^{III}\cdots$Mn^{III}) using the Hamiltonian H = -2J**S**$_1$**S**$_2$. The best fit gave a value of $J_{bb} = 1.0$ cm^{-1} with $g = 2.00$ (Fig. 2, red line). The J parameter

results in an $S = 4$ ground state, with excited states 39.2 cm^{-1} ($S = 3$) above the ground. The best fit for compound **3**, reported using an H = -2J**S**$_1$**S**$_2$ Hamiltonian, yielded a J parameter of 3.4 cm^{-1} ($g = 2.14$) and an $S = 4$ spin ground state.[10]
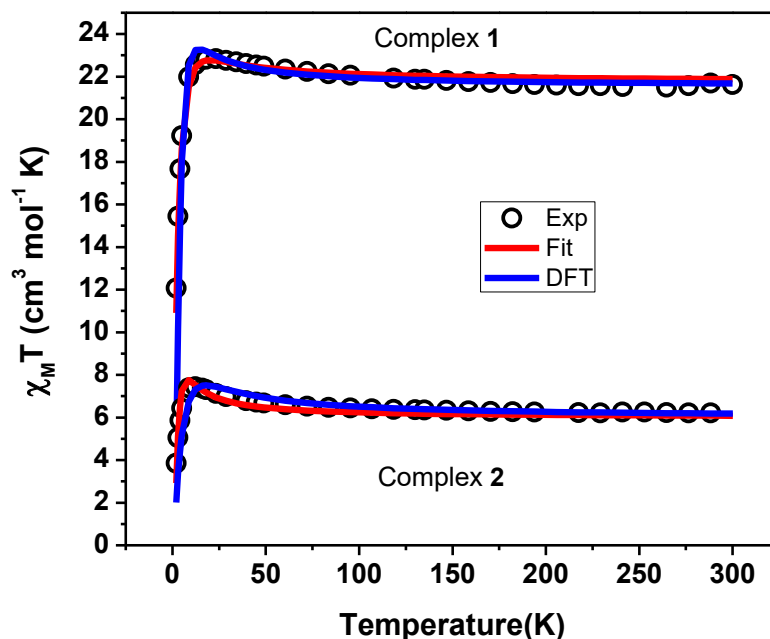
Fig. 2. Plots of $\chi_M T$ versus T for **1** and **2** in the temperature range 2 – 300 K in a dc field of 1 T.

The observed *M vs H* data for **1**–**2** are shown in Fig. 3. Poor fits were obtained using the exchange-only models (Eqns 1 and 2) and J values deduced by susceptibility fitting, particularly at high fields (Fig. 3 top figures). The magnetization data were then fitted (Fig. 3, bottom) using the giant spin model to extract the D values of Mn(III) ions and the exchange parameters (Eqns 3 and 4) with very good fits obtained.
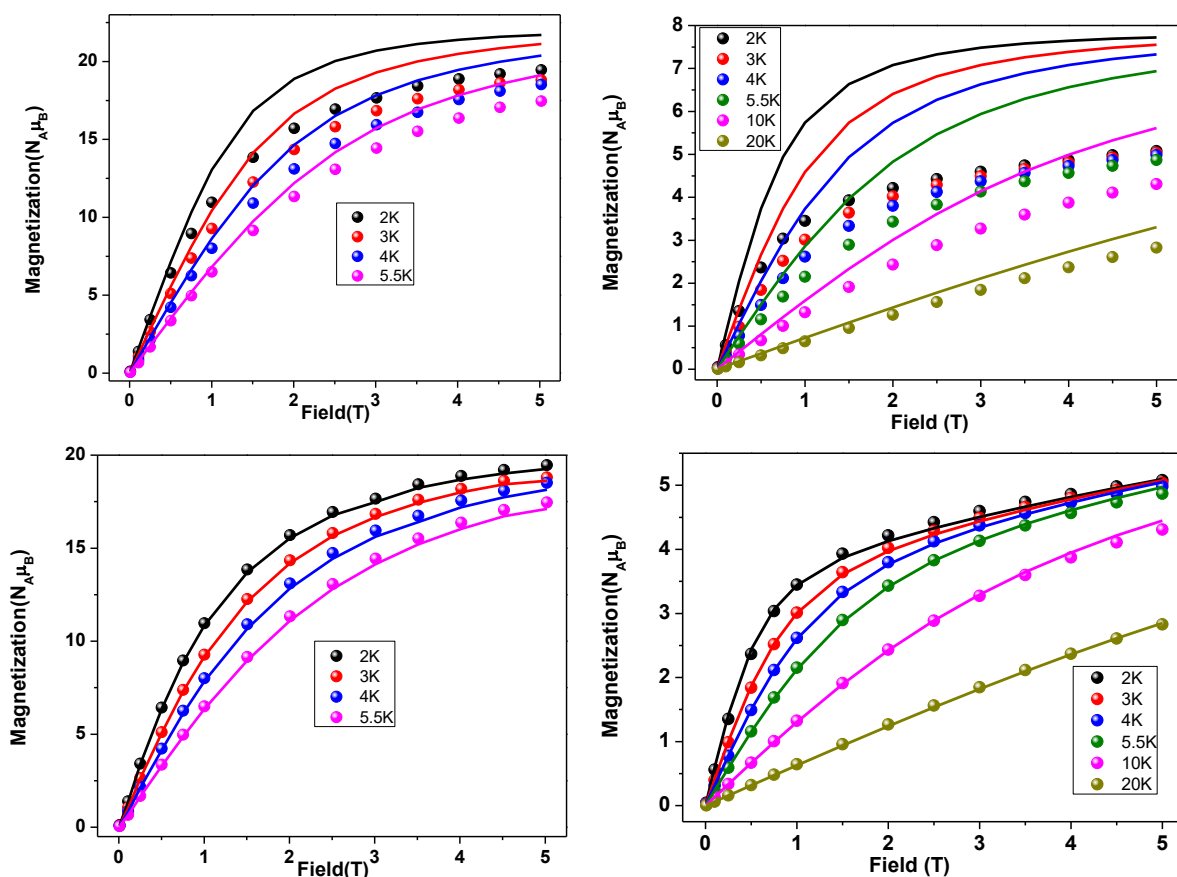
The following Hamiltonian was used for complex **1**.

$$\widehat{H} = -[2J_{wb}(S_{Mn1} S_{Gd1} + S_{Mn1} S_{Gd1'} + S_{Mn1'} S_{Gd1} + S_{Mn1'} S_{Gd1'}) + 2J_{bb}(S_{Mn1} S_{Mn1'})$$
$$+ 2J_{ww}(S_{Gd1} S_{Gd1'})] + D_{Mn}S_z^2 + \mu_B g_{Mn} H.S \qquad Eq.3$$

The following Hamiltonian was used for complex **2**.

$$\widehat{H} = -2J_{bb}(S_{Mn1} S_{Mn1'}) + D_{Mn}S_z^2 + \mu_B g_{Mn} H.S \qquad Eq.4$$

Fig. 3. *M* vs. *H* isotherms for (left) **1** and (right) **2** at temperatures 2 (top), 3, 4, 5.5, 10 and 20 (bottom) K. (both top figures): the solid lines are simulated data to validate the exchange parameters obtained from the susceptibility data. (both bottom figures): the solid lines are fitted data obtained from the giant spin model Hamiltonian. See below for the discussion.

The best fit values yielded J_{bb} = 7.11 cm^{-1}, J_{wb} = 0.01 cm^{-1} and D_{Mn} = -3.25 cm^{-1} with g = 1.81 (Figure 4, bottom left) for complex **1**. For complex **2**, the best fit gave a value of J_{bb} = 2.55 cm^{-1} with g = 1.76 (Figure 4, bottom right) and a D_{Mn} value of -3.42 cm^{-1}. These J parameters are slightly larger than the J values extracted using the susceptibility data. However, the ferromagnetic coupling constants still result in an S = 11 ground state for complex **1** and S = 4 ground state for complex **2**. The g values are smaller than the value of 2.0, which is sometimes noted in Mn^{III} clusters [6,7]. Here, since this is the g-tensor obtained for the ground state S =11, in **1**, arising from coupling of spins between Gd(III) and Mn(III) ions, this could be justified The D_{Mn} values are in line with those expected for anisotropic Mn^{III} ions with the Jahn–Teller distorted octahedral geometries. [8]

Theoretical Studies

Computational methods are essential in calculating the magnetic properties of paramagnetic complexes [12,13,14,22]. Even though extensive experimental studies have been performed on many {3d-4f} systems, only a limited number of theoretical studies have been explored [23-26] particularly in the estimation of magnetic exchange interaction J and in understanding the mechanism of magnetic coupling. We have therefore undertaken a theoretical analysis to calculate all the possible exchange interactions in **1–3**. Moreover, we attempt to rationalize why the Mn^{III}-Mn^{III} superexchange interaction is ferromagnetic in complexes **1 – 3**.

Comparison of experimental and DFT calculated data.
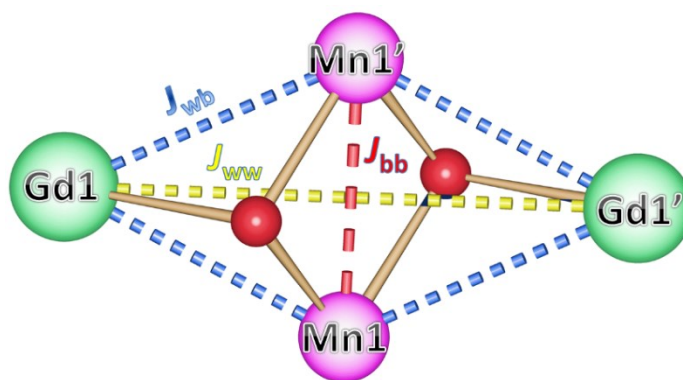
Fig. 4. Magnetic exchange pathways in **1 – 3** (Three Js for **1** and only J_{bb} for **2** and **3**).

In order to explore the magnetic properties, fitting of the experimental magnetic data was performed using the PHI program [21], as described above, in order to extract the nature and the magnitude of the magnetic exchange interactions within each cluster. It is often found that only two J values (J_{bb} and J_{wb} (Fig.4)) are generally reported in the literature, due to the complications of performing fits with many J values (see Table 1) and thus the J_{ww} interaction has been neglected in this study for **1**. Since the lanthanides are diamagnetic in **2** and **3** we have fitted the experimental magnetic data for the exchange between Mn^{III} ions only (J_{bb}). The exchange topology used to calculate the J values is shown in Fig. 4.

Table 1: Experimental susceptibility and DFT deduced exchange coupling constants (J values) for **1**–**3**. J_{exp} is the same as FIT in Fig. 3

Complex	J_{exp}(cm^{-1})		J_{DFT}(cm^{-1})		
	J_{bb}	J_{wb}	J_{bb}	J_{wb}	J_{ww}
1	1.7	0.014	1.2	0.06	-0.0002
2	1.0		1.9		
3	3.4		4.2		

In **1-3** both the experimentally fitted parameters (FIT in Fig. 2) and the DFT calculated values reveal a ferromagnetic interaction for the J_{bb} interaction with a small variation in the magnitude. In **1**, both the $\chi_M T$ fitted parameter and the DFT calculations predict a very weak ferromagnetic J_{wb} value (Table 1). From DFT the J_{ww} interaction is found to be negligible and antiferromagnetic for **1**. The temperature dependence of $\chi_M T$ for the DFT calculated J values with the inclusion of small $zJ = -0.01$ cm^{-1} provides excellent fits to the experimental data for **1**–**3** (see Figs. 2 and S4).

Mn^{III}-Mn^{III} superexchange (J_{bb}): We earlier reported that the dihedral angle between J-T axes in {Mn$^{III}_2$(OR)$_2$} complexes to be the prominent parameter in controlling the sign and magnitude of exchange [8b,c]. The {Mn$^{III}_2$(OR)$_2$} core in complexes **1-3** have a similar topology to the studied dinuclear systems each of which has parallel J-T axes on the Mn^{III} ions and parallel to the bridging plane. This situation here belongs to the type-II manganese dinuclear complexes as previously reported [8b,c]. In general, type-II complexes (Fig. 5) exhibit weak ferro- and antiferromagnetic exchange interactions (-1.7 to $+6.3$ cm^{-1}) [8c] and here we observe weak ferromagnetic interactions. The J-T axes are present along the Mn-O-Mn-O direction which results in a significant $|d_z^2-d_{x^2-y^2}|$ cross-interaction leading to a larger J_F term. Moreover, the Mn-O-Mn angles are relatively smaller (~97 degrees) compared to the dinuclear {Mn$^{III}_2$(OR)$_2$} complexes previously reported [8] which results in a moderate antiferromagnetic interaction due to a weak overlap of the dxz|dxz and dyz|dyz orbitals (see Table S3). The dominant J_F term therefore leads to net ferromagnetic J for Mn^{III}-Mn^{III} exchange in all three complexes studied here.
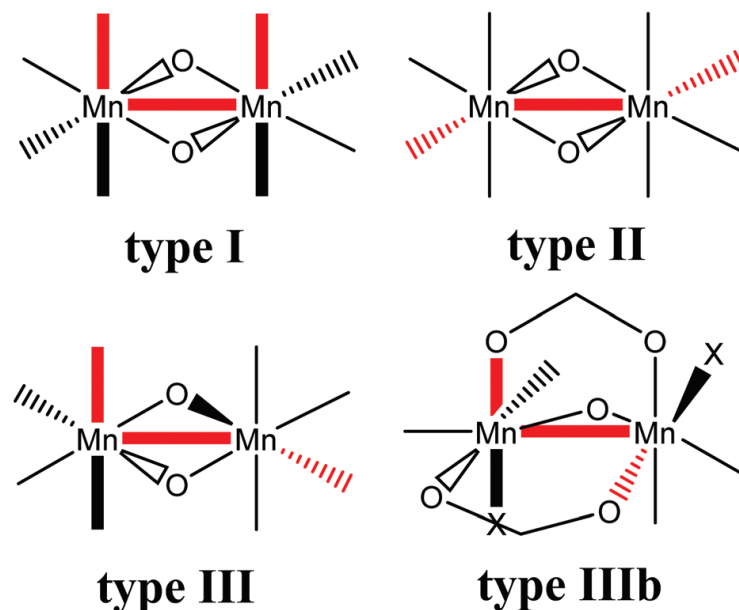
Fig. 5. Schematic illustrating the three types (I–III) of J-T orientations observed in previously reported μ-OR bridged [Mn^{III}_2] dimers [8c]. The red/black bold lines show the JT dihedral angle.

Mn-Gd coupling (J_{wb}) in 1: The unpaired electron in the d_z^2 orbital of the Mn^{III} ions is likely to play a pivotal role both in contributing to the J_F term, via charge-transfer, and also as a σ-type orbital overlaping with the 4f orbitals of Gd^{III} thereby contributing to the J_{AF} term [27]. However 3d-4f orbital overlaps are generally weak and dominating terms are the charge transfer from the 3d to the Gd(III) 5d orbital [28]. In particular, the presence of an unpaired electron in the d_z^2 orbital helps to enhance this charge transfer leading to ferromagnetic interaction for the {Mn^{III}-Gd^{III}} pair as we have shown earlier [14a]. Thus the dominating charge transfer mechanism lead to ferromagnetic coupling. However, as the J-T axes of the Mn^{III} ions are parallel to the {$MnGdO_2$} plane, leading to less efficient overlap, and hence a weak ferromagnetic coupling, as computed.

It is interesting to compare the J_{bb} and J_{wb} values deduced for **1** with those for a related butterfly complex [$Mn^{III}_2Gd^{III}_2(μ_3\text{-}O)_2(O_2C^tBu)_{10}$][$Et_3NH$]$_2$, the latter containing μ$_3$-O bridges whereas **1** contains μ$_3$-OMe bridges [29]. The J_{bb} value for this μ-oxo complex was found to be -58 cm^{-1} while J_{wb} was +5.5 cm^{-1}, the large difference in size and sign to **1** ascribed to the Mn-O-Mn bridging motif [29] and attendant geometric differences, with spin density effects of the type described below not reported but probably important.

Spin density and ground state analysis:
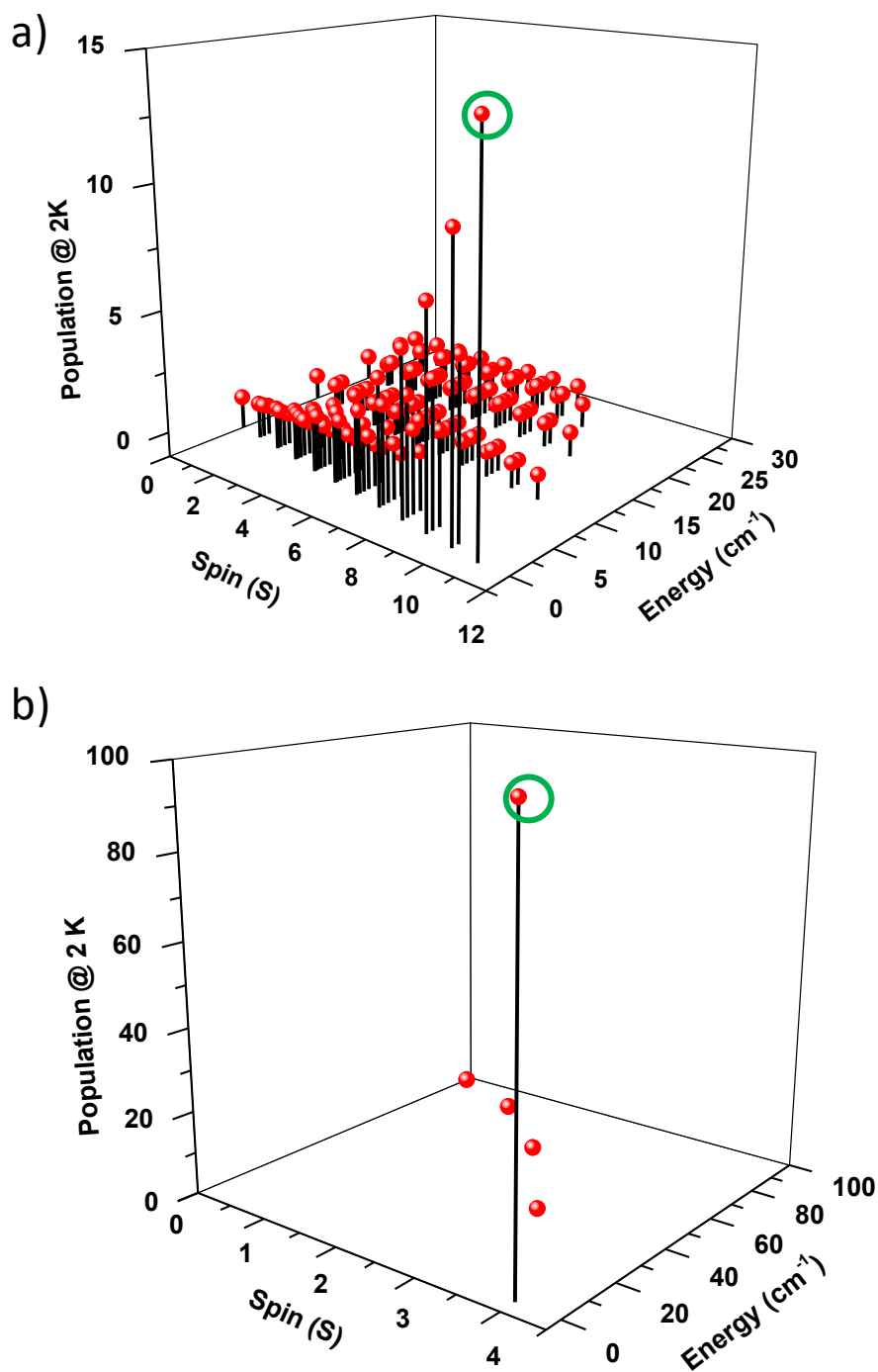
Fig. 6. Eigenvalue plot of complex (a) **1** for $S = 11$ spin state (c) **2** for $S = 4$ spin state. A similar diagram is applicable for complex **3** (ground state highlighted).

The experimentally fitted J values and the DFT computed J values (see Fig.6a) yields an $S = 11$ ground state for complex **1**. The ground state spin density plot for $S = 11$ (DFT calculated) is shown in Fig. 7a. The $S = 11$ ground state can be achieved when all Mn(III) and Gd(III) ions are spin-up. Spin delocalization is observed for the Mn^{III} ions (spin density of ~3.84) and

spin polarization is observed for the Gd^{III} ions (~7.03). The central μ_3-O atoms gain a spin density of 0.02 via spin delocalization.
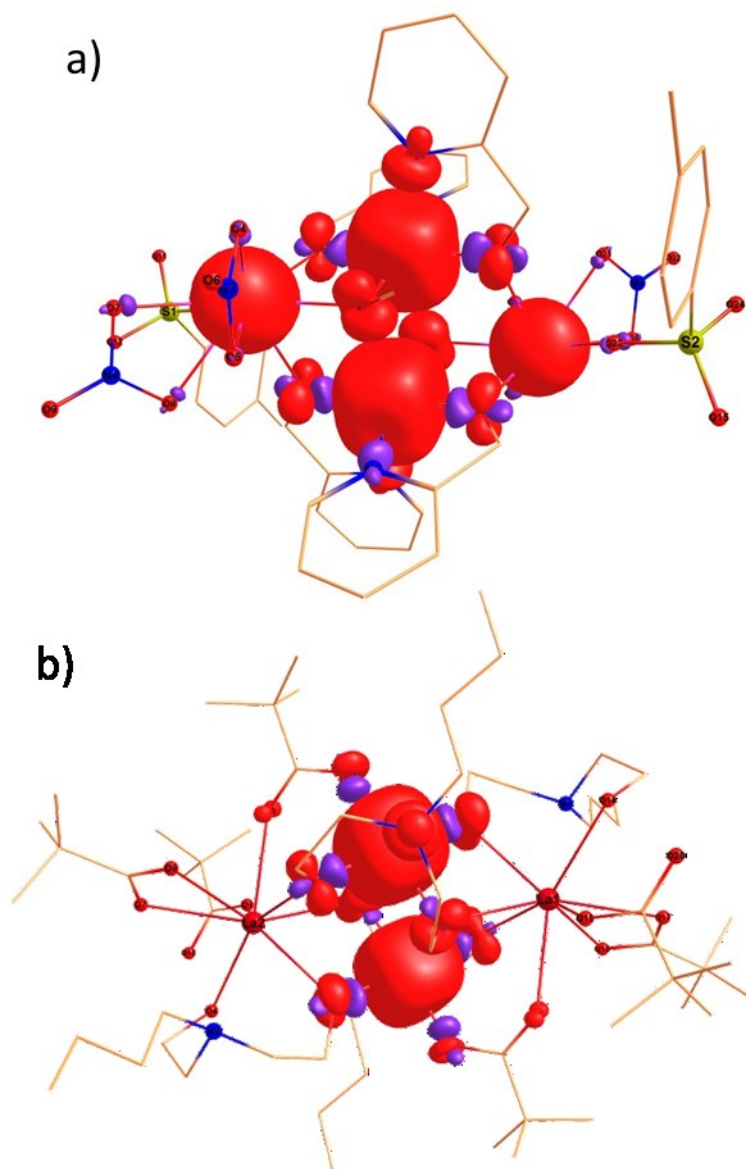
Fig. 7. Spin density plot of complex a) **1** ($S = 11$) and b) **3** ($S = 4$). A similar spin-density diagram to that in b) is applicable for complex **2**.

For complexes **2** and **3**, the experimentally fitted and DFT computed J values result in an $S = 4$ ground state (see Fig. 6b). The spin ground state $S = 4$ for complex **2** and **3** is achieved when both body Mn^{III} ions have spin-up. The spin density plot for $S = 4$ is shown in Fig. 7b. Spin delocalization is observed for the Mn^{III} ions (spin density of ~3.84). The central μ_3-O

atoms display a spin density of (0.03) and the diamagnetic lanthanides gain a spin density (0.01) via spin polarization.

Conclusions

Three $\{Mn^{III}_2Ln^{III}_2\}$ (Ln = Gd (**1**), Y (**2**) and La (**3**)) butterfly complexes bearing μ-alkoxo bridged Mn^{III} dinuclear moieties have been synthesised, structurally and magnetically characterized with the magnetic properties analysed using DFT calculations. Using a previously reported classification scheme to rationalize the magnetic exchange parameter for dinuclear Mn^{III} complexes, [8b, c] **1 – 3** are classed as type-II Mn^{III} dinuclear complexes. Type-II complexes reveal parallel Jahn-Teller axes on the Mn^{III} ions which lie parallel to the bridging plane. The Mn^{III}-Mn^{III} magnetic exchange interaction shows weak ferromagnetic coupling. The sign of the fits of the experimental susceptibility data of the Mn^{III}-Mn^{III} interaction are in good agreement with the DFT calculated parameters for **1** [1.7 cm^{-1} (1.2 cm^{-1})], **2** [1.0 cm^{-1} (1.9 cm^{-1})] and **3** [3.4 cm^{-1} (4.2 cm^{-1})], with a small variation in magnitude. The agreement is not as good using the giant Spin model to fit magnetisation isotherms though the signs of J_{MnMn} are the same. The spin ground state values for **1 – 3** are $S = 11$, $S = 4$ and $S = 4$, respectively, using both fitting methods. In **1**, the excited spin states are very close in energy to the ground state. We, therefore, show that it is possible to isolate a large spin ground state with parallel J-T axes which will result in a significant magnetic anisotropy, important in future SMM design.

Acknowledgements

References

[1] D. N. Woodruff, R. E. P. Winpenny, R. A. Layfield, Chem. Rev. 113 (2013) 5110.

[2] J. Tang, P. Zhang, Lanthanide Single Molecule Magnets, Springer-Verlag, Berlin, 2015.

[3] D. Gatteschi, R.Sessoli, J. Villain, Molecular Nanomagnets, Oxford University Press,

U. K., 2011.

[4] G. Christou, Polyhedron, 24 (2005) 2065.

[5] recent high T_B example: a) C. A. P. Goodwin, F. Ortu, D. Reta, N. F. Chilton, D. P. Mills, Nature, 548 (2017) 439; b) F.-S. Guo, B. M. Day, Y.-C. Chen, M.-L. Tong, A. Mansikkamäki, R. A. Layfield, Science, 362 (2018) 1400.

[6] K. S. Murray, Adv. Inorg. Chem., 43 (1995) 261.

[7] L. Wittick, K.S. Murray, B. Moubaraki, S.R. Batten, L. Spiccia, K.J. Berry, Dalton Trans., 0 (2004) 1003.

[8] a) K. R. Vignesh, S. K. Langley, K. S. Murray, G. Rajaraman, Chem. Eur. J. 21 (2015) 2881; b) K. R. Vignesh, S. K. Langley, C. J. Gartshore, I. Borilović, .C M. Forsyth, G. Rajaraman, K. S. Murray, Dalton Trans., 47 (2018) 11820; c) N. Berg, T. Rajeshkumar, S. M. Taylor, E. K. Brechin, G. Rajaraman and L. F. Jones, Chem. Eur. J., 18 (2012) 5906.

[9] S. K. Langley, B. Moubaraki, K. S. Murray, Austral. J. Chem. 67 (2014) 1601.

[10] M. N. Akhtar, Y. Lan, V. Mereacre, R. Clerac, C. E. Anson, A. K. Powell, Polyhedron 28 (2009) 1698.

[11] L. Noodleman, J. Chem. Phys., 74 (1981) 5737.

[12] a) E. Ruiz, S. Alvarez, A. Rodriguez-Fortea, P. Alemany, Y. Pouillon, C. Massobrio, in J. S. Miller, M. Drillon (Eds), Magnetism: Molecules to Materials, Vol. II Wiley-VCH, Weinheim, 2001, p. 227; b) S. Piligkos, G. Rajaraman, M. Soler, N. Kirchner, J. van Slageren, R. Bircher, S. Parsons, H. Güdel, J. Kortus, W. Wernsdorfer, G. Christou, E. K. Brechin, J. Am. Chem. Soc., 127 (2005) 5572; c) P. Christian, G. Rajaraman, A. Harrison, M. Helliwell, J. J. W. McDouall, J. Raftery, R. E. P. Winpenny, Dalton Trans., 0 (2004) 2550.

[13] a) G. Rajaraman, M. Murugesu, E. C. Sanudo, M. Soler, W. Wernsdorfer, M. Helliwell, C. Muryn, J. Raftery, S. J. Teat, G. Christou, E. K. Brechin, J. Am. Chem. Soc., 126 (2004) 15445; b) G. Rajaraman, G., E . Ruiz, J. Cano, S. Alvarez, Chem. Phys. Lett., 415 (2005) 6; c) P. Christian, G. Rajaraman, A. Harrison, J. J. W. McDouall, J. T. Raftery, R. E. P. Winpenny, Dalton Trans., 0 (2004) 1511; d) G. Rajaraman, J. Cano, E.

K. Brechin, E. J. L.McInnes, Chem. Commun., 0 (2004) 1476; e) K. R. Vignesh, S. K. Langley, C. J. Gartshore, B. Moubaraki, K. S. Murray, G. Rajaraman, Inorg. Chem., 56 (2017) 1932.

[14] a) M. M. Hanninen, A. J. Mota, R. Sillanpaa, S. Dey, G. Velmurugan, G. Rajaraman, E. Colacio, Inorg. Chem., 57 (2018) 3683; b) S. De, S. Tewary, D. Garnier, Y. Li, G. Gontard, L. Lisnard, A. Flambard, F. Breher, M-L. Boillot, G. Rajaraman. R. Lescoueze, Eur. J. Inorg. Chem., 57 (2018) 414; c) K. R. Vignesh, S. K. Langley, B. Moubaraki, K. S. Murray, G. Rajaraman, Inorg. Chem., 57 (2018) 1158; d) T. Gupta, G. Rajaraman, Chem. Commun., 52 (2016) 8972; e) K. R. Vignesh, S. K. Langley, B. Moubaraki, K. S. Murray, G. Rajaraman, Chem. Eur. J., 21 (2015) 16364.

[15] A. D. Becke, J. Chem. Phys., 98 (1993) 5648.

[16] M. J. Frisch, G. W. Trucks, H. B. Schlegel, G. E. Scuseria, M. A. Robb, J. R. Cheeseman, G. Scalmani, V. Barone, B. Mennucci, G. A. Petersson, H. Nakatsuji, M. Caricato, X. Li, H. P. Hratchian, A. F. Izmaylov, J. Bloino, G. Zheng, J. L. Sonnenberg, M. Hada, M. Ehara, K. Toyota, R. Fukuda, J. Hasegawa, M. Ishida, T. Nakajima, Y. Honda, O. Kitao, H. Nakai, T. Vreven, J. A. Montgomery, J. E. Peralta, F. Ogliaro, M. Bearpark, J. J. Heyd, E. Brothers, K. N. Kudin, V. N. Staroverov, R. Kobayashi, J. Normand, K. Raghavachari, A. Rendell, J. C. Burant, S. S. Iyengar, J. Tomasi, M. Cossi, N. Rega, J. M. Millam, M. Klene, J. E. Knox, J. B. Cross, V. Bakken, C. Adamo,J. Jaramillo, R. Gomperts, R. E. Stratmann, O. Yazyev, A. J. Austin, R. Cammi, C. Pomelli, J. W. Ochterski, R. L. Martin, K. Morokuma, V. G. Zakrzewski, G. A. Voth, P. Salvador, J. J. Dannenberg, S. Dapprich, A. D. Daniels, O. Farkas, J. B. Foresman, J. V. Ortiz, J. Cioslowski, D. J. Fox, Gaussian, Inc., Gaussian 09, Revision A.02, Wallingford CT, 2009.

[17] T. R. Cundari, W. J. Stevens, J. Chem. Phys., 98 (1993) 5555.

[18] (a) T. H. Dunning Jr. and P. J. Hay, H. F. Schaefer III, ed., PLENUM PRESS (1977); (b) P. J. Hay and W. R. Wadt, J. Chem. Phys., 82 (1985) 270; (c) P. J. Hay and W. R. Wadt, J. Chem. Phys., 82 (1985) 284; (d) P. J. Hay and W. R. Wadt, J. Chem. Phys., 82 (1985) 299.

[19] a) A. Schafer, H. Horn, R. Ahlrichs, J. Chem. Phys. 97 (1992) 2571; b) A. Schafer, C. Huber, R. Ahlrichs, J. Chem. Phys. 100 (1994) 5829.

[20] A. Bencini, F. Totti, Int. J. Quantum Chem., 101 (2005) 819-825.

[21] N. F. Chilton, R. P. Anderson, L. D. Turner, A. Soncini, K. S. Murray, J. Comput. Chem. 34 (2013) 1164.

[22] K. Hegetschweiler, B. Morgenstern, J. Zubieta, P. J. Hagrman, N. Lima, R. Sessoli, F. Totti, Angew. Chem. Int. Ed., 43 (2004) 3436.

[23] I. Rudra, C. Raghu, S. Ramasesha, Phys Rev. B., 65 (2002) 224411.

[24] a) E. Ruiz, T. Cauchy, J. Cano, R. Costa, J. Tercero, S. Alvarez, J. Am. Chem. Soc., 130 (2008) 7420; b) E. Ruiz, J. Cirera, J. Cano, S. Alvarez, C. Loose, J. Kortus, Chem. Comm., 1 (2008) 52; c) E. Ruiz, Struct. Bond. Springer, Berlin, Germany, 113 (2004) 71.

[25] J. Kortus, M. R. Pederson, T. Baruah, N. Bernstein, C. S. Hellberg, Polyhedron, 22 (2003) 1871.

[26] G. Rajaraman, F. Totti, A. Bencini, A. Caneschi, R. Sessoli, D. Gatteschi, Dalton Trans., (2009) 3153.

[27] S. K. Singh, T. Rajeshkumar, V. Chandrasekhar, G. Rajaraman, Polyhedron, 66 (2013) 81.

[28] a) S. K. Singh, G. Rajaraman, Dalton Trans., 42 (2013) 3623; b) S. K. Singh, N. K. Tibrewal, G. Rajaraman, Dalton Trans., 40 (2011) 10897.

[29] E. Moreno Pineda, N. F. Chilton, F. Tuna, R.E. P. Winpenny, E. J. L. McInnes, Inorg. Chem., 54 (2015) 5930.

Captions to Figures

Fig. 1: (a) Molecular structure of **1** (Same applicable to **2**); (b) Molecular structure of **3** [10]. Mn^{III}, pink; Gd^{III}, green; La^{III}, orange;O, red; N, blue; C, black; S, yellow. The black bold bonds denote the Mn^{III} J-T axes which are elongated via O-Mn-N.

Fig. 2. Plots of $\chi_M T$ versus T for **1** and **2** in the temperature range $2 - 300$ K in a dc field of 1 T.

Fig. 3. M vs. H isotherms for (left) **1** and (right) **2** at temperatures 2 (top), 3, 4, 5.5, 10 and 20 (bottom) K. (both top figures): the solid lines are simulated data to validate the exchange parameters obtained from the susceptibility data. (both bottom figures): the solid lines are fitted data obtained from the giant spin model Hamiltonian. See below for the discussion.

Fig. 4. Magnetic exchange pathways in **1 – 3** (Three Js for **1** and only J_{bb} for **2** and **3**)

Fig. 5. Schematic illustrating the three types (I–III) of J-T orientations observed in previously reported μ-OR bridged $[Mn^{III}_2]$ dimers [8c]. The red/black bold lines show the JT dihedral angle.

Fig. 6. Eigenvalue plot of complex (a) **1** for $S = 11$ spin state (c) **2** for $S = 4$ spin state. A similar diagram is applicable for complex **3** (ground state highlighted).

Fig. 7. Spin density plot of complex a) **1** ($S = 11$) and b) **3** ($S = 4$). A similar spin-density diagram to that in b) is applicable for complex **2**.